ELSEVIER

Journal of Fluids and Structures 19 (2004) 321–334

JOURNAL OF FLUIDS AND STRUCTURES

www.elsevier.nl/locate/jnlabr/yjfls

Experimental investigation of the mean and fluctuating forces of wavy (varicose) cylinders in a cross-flow

K. Lam[a,*], F. H. Wang[b], J.Y. Li[b], R.M.C. So[a]

[a] *Department of Mechanical Engineering, The Hong Kong Polytechnic University, Hung Hom, Kowloon, Hong Kong*
[b] *School of Energy and Power Engineering, Xi'an Jiaotong University, Xi'an, PR China*

Received 4 March 2002; accepted 20 December 2003

Abstract

The effects of surface waviness of wavy (varicose) cylinders on mean drag and fluctuating lift reduction were experimentally investigated. The experiments were carried out in a low speed wind tunnel having a $0.6\,\mathrm{m} \times 0.6\,\mathrm{m}$ cross-section and a free-stream turbulence intensity less than 0.2%. The Reynolds numbers, based on the free-stream velocity and the nominal cylinder diameter, vary from about 2.0×10^4 to 5.0×10^4. Measurements on mean and fluctuating forces induced by a cross-flow over three wavy cylinders and the circumferential pressure distributions at various spanwise positions are presented. From these results, it can be concluded that the mean drag coefficients of the wavy cylinders are less than that of a corresponding circular cylinder; a drag reduction of up to 20% was obtained. It was also found that the root-mean-square fluctuating lift coefficients of the wavy cylinders are much lower than those of a circular cylinder. However, the spectral analysis of both hot-wire and load cell signals show that the Strouhal numbers of the wavy cylinders are essentially the same as a corresponding circular cylinder.

Keywords: Wavy cylinders; Vortex shedding; Fluctuating force; Drag reduction

1. Introduction

Bluff bodies are found in many engineering applications, including heat exchangers, risers in marine engineering, road vehicles, buildings and bridges. Vortex shedding in their wake can generate large unsteady forces, which have the potential to damage the structural integrity of the bluff bodies. For this reason, many methods have been proposed over recent years to control the dynamics of the wake vortices with the aim of suppressing vortex shedding and reducing the fluctuating lift force as well as the magnitude of the mean drag force.

Blevins (1994) pointed out that the reduction of vortex-induced vibration on bluff bodies could be achieved (i) by increasing reduced damping, (ii) by avoiding resonance, (iii) by streamlining the cross-section, or (iv) by adding a vortex suppression device. However, in many situations, the first three methods are not suitable; therefore, the fourth method is often used in practice. For example, vibration reduction could be achieved by adding helical strakes, a perforated shroud, axial slats, a splitter plate, ribbon cable, pivoted guiding vane and spoiler plates. The principles of these devices are either to effect suppression of the strength of the shed vortex or to suppress the spanwise correlation of the shed vortex, thus causing three dimensionality. Nuzzi et al. (1992) studied the three-dimensional vortex formations from a nonuniform cylinder, while Hover et al. (1998) investigated the forces on a uniform and a tapered cylinder.

*Corresponding author. Tel.: +852-27666649; fax: +852-23654703.
E-mail address: mmklam@polyu.edu.hk (K. Lam).

0889-9746/$ - see front matter © 2004 Elsevier Ltd. All rights reserved.
doi:10.1016/j.jfluidstructs.2003.12.010

In many cases, reduction of the mean drag force on bodies is important to engineering applications, e.g., the flow around cylindrical tubes in heat exchangers and the flow around certain airfoils at large incidence angles. Various methods have been used to reduce the mean drag force of bluff bodies in a cross-flow by disturbing the flow field around the bodies or by changing the structure of the shed vortices. For example, the method using base bleed or a splitter plate could increase the base pressure and thus reduce the drag force on the bluff bodies. The influences and mechanisms of these techniques are well understood.

Besides the methods mentioned above, some new approaches have been proposed and examined carefully. Sakamoto and Haniu (1994) put forward one such method. They reported their findings on the optimum suppression of fluid forces acting on a circular cylinder by placing a small cylinder upstream, and found that a reduction of the mean drag force up to 50% was achievable. Another method is to introduce three-dimensional geometric disturbances that interfere with and weaken regular vortex shedding. It is mainly used to reduce the mean drag of wings with blunt trailing edges. There are two ways to achieve this. One is to use segmented trailing edges. The effect of geometry on the base pressure recovery of segmented blunt trailing edges was investigated by Petrusma and Gai (1994), while a comparison experiment was carried out by Petrusma and Gai (1996) to examine the bluff body wake with free, fixed, and discontinuous separation. Bearman (1965) found that the decrease of base drag with an increase of formation length has been linked to the curvature of the separated shear layer. Hence, the increase in formation length led to a reduction of the suction near the base of the cylinder and this gave rise to a reduction of the mean drag. On the other hand, Tombazis and Bearman (1997) were interested in the large-scale three-dimensional features found in the wakes of nominal two-dimensional bluff bodies and their effects on drag reduction. Rodriguez (1991) studied the drag reduction by controlling the three-dimensional unsteady vortical structures. Bearman and Tombazis (1993) investigated the three-dimensional features of the wake behind a blunt-base model with a wavy trailing edge. They founded that by increasing the wave steepness, the base pressure was increased with a concomitant decrease in drag. Recently, Bearman and Owen (1998) proposed using such a method in thin plates and obtained a drag reduction of up to 30%.

Among the drag reduction methods mentioned above, many are not omni-directional. Furthermore, some of them cannot reduce drag and suppress structural vibration simultaneously. The present investigation aims to seek a method that could reduce drag and fluctuating lift simultaneously. One such proposal is a cylinder with a three-dimensional surface geometry. The geometry chosen for investigation is a wavy cylinder (Fig. 1). This geometry is selected because it is a natural three-dimensional extension of the well-documented right circular cylinder. Moreover, it is omni-directional. It is anticipated that the wavy cylinder, if designed properly, could reduce the mean drag and the associated fluctuating lift.

Numerous studies have been carried out on flow around wavy cylinders. Davey (1961) studied the flow of a viscous incompressible fluid in the immediate neighborhood of a saddle point of attachment. Cooke and Robins (1970) solved

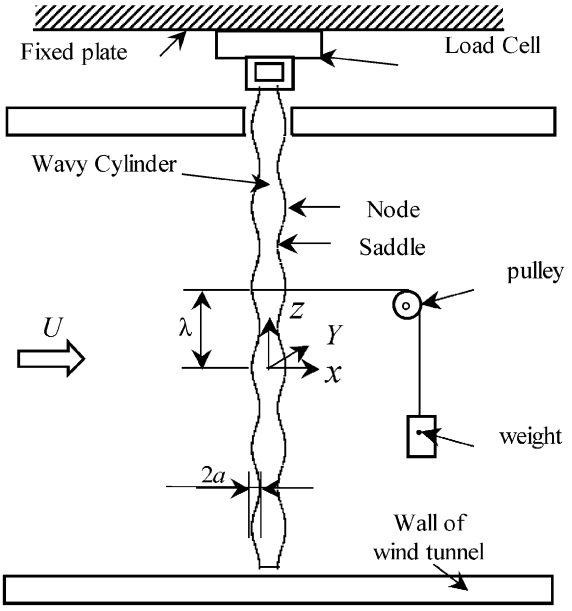

Fig. 1. Geometry and coordinate system of the wavy cylinders.

the boundary layer flow between nodal and saddle points of attachment using a finite difference method. On the other hand, Duck (1979) investigated the flow induced by a torsionally oscillating wavy cylinder at a Taylor number close to its critical value, and the interaction between the forced and natural solutions. The results of the above investigations show that for sufficiently small waviness the entire boundary layer flow from the geometric nodal point to the geometric saddle point is without separation. Kerczek (1988) predicted that a reversed flow would occur (directed away from the saddle and towards the nodal point), but that it would be limited to the bottom of the boundary layer. It would not disrupt the outer flow, though. Keser et al. (2001) used a three-dimensional discrete vortex method to simulate the separated flow around a circular cylinder with sinusoidal waviness along its span. All the above efforts were based on various assumed forms for the pressure distribution from the nodal to the saddle point of attachment, since there were no prior experimental data available for the pressure distribution over a wavy cylinder.

In the experimental area, Ahmed and Bays-Muchmore (1992) measured the surface-pressure distributions of a set of wavy cylinders with different axial wavelengths based on the mean cylinder diameter. Their results showed that the separated flow structures near the geometric nodes were distinctly asymmetric for a large fraction of time and the sectional drag coefficients at the geometric nodes are greater than at the geometric saddle. In another study, Ahmed et al. (1993) explored the effects of the three-dimensional separation line topology on the development of the wavy turbulent wake. They also presented and analyzed the mean velocity field and the Reynolds stresses. As a result, they found that the formation of trailing streamwise vortices behind nodal points of separation gave rise to a locally narrower wake, a rapid wake velocity recovery and a suppression of the turbulence development within the separated boundary layer. They further found that the Reynolds stress field in the immediate wake exhibited large spanwise variations. The mean drag force acting on a wavy cylinder has also been measured by Ahmed and Bays-Muchmore (1992) using surface pressure taps. The Reynolds number in their experiment was 2.0×10^4 and the mean static pressure distribution data was determined using linear interpolation.

The above brief review shows that the flow fields behind wavy cylinders have been extensively examined. However, other important parameters, such as the lift and drag coefficients, the vortex shedding frequency and the associated Strouhal number, have not been thoroughly examined. Furthermore, whether the wavy cylinder is capable of suppressing the fluctuating lift and concomitantly reducing the mean drag force is not known. Therefore, the purpose of this study is to investigate the mean and fluctuating forces on wavy cylinders subjected to a cross-flow. The static pressure distribution along the span of the cylinder, the mean force, spanwise averaged fluctuation forces, and the vortex shedding frequencies are systematically measured. A brief description of the experimental set-up including the wind tunnel loop and the techniques used in the experiment is given in Section 2. The experimental results are discussed in Section 3. Finally, Section 4 summarizes the conclusions drawn from these results.

2. Experimental set-up and measurement techniques

2.1. Wind tunnel facility

The facility used in this experiment is a closed circuit wind tunnel with a working square cross-section (0.6 m × 0.6 m) and a length of 2.0 m. The test-section is made of Perspex. The velocity in the test-section could be continuously varied from 0 to 40 m/s by an inverter, which controls the rotation speed of the wind tunnel fan. The boundary layer on the wall at the location where the cylinder was introduced was measured to be about 20 mm thick, while the free-stream turbulent intensity was measured to be less than 0.2%. The maximum blockage in the experiments is about 4%. A standard Pitot-static tube connected to an electronic micromanometer, made by Furness Contol Limited, was installed in the wind tunnel to monitor the inlet free-stream velocity.

2.2. Model geometry and set-up

The terminology used to describe the wavy cylinders is defined in Fig. 1. The axial locations of the maximum diameter are hereafter termed "nodes", while the axial locations of the minimum diameter are denoted "saddles". Three different wavy cylinders were used in the wind tunnel experiments. The geometry of the wavy cylinders is described by the equation, $D_z = D_{\text{mean}} + 2a\cos(2\pi z/\lambda)$. Here, D_z is the local diameter, D_{mean} is the mean diameter, a is the amplitude of the surface curve, λ is the wavelength, and z is the spanwise location. It is obvious that the surface geometry of the wavy cylinder can be defined by two parameters: one is the normalized amplitude, a/D_{min}, and the other is the normalized wavelength, λ/D_{min}. However, neither of them alone can express the cylinder geometry accurately. In this investigation, we combine the two parameters into one normalized parameter to represent the surface waviness.

Table 1
Geometrical parameters and dynamic characteristics of the test cylinders

Parameters	Wavy cylinder Model 1	Wavy cylinder Model 2	Wavy cylinder Model 3
The minimum diameter $D_{\min}$ (mm)	18	18	18
The maximum diameter $D_{\max}$ (mm)	26	26	30
Amplitude a (mm)	2	2	3
Wavelength λ (mm)	32	50	50
Length L (mm)	598.5	598.5	598.5
$a^2/(\lambda D_{\min})$	0.00694	0.00444	0.01002
Natural frequency first mode f_{n1}	9 Hz	12 Hz	7 Hz
Natural frequency first mode f_{n2}	92 Hz	97 Hz	90 Hz
Natural frequency first mode f_{n3}	273 Hz	278 Hz	233 Hz
Damping ratio ζ	0.0177	0.0454	0.0549
Mass ratio $m/\rho D_{\text{mean}}^2$	5722	5795	5963
Reduced damping $\frac{1}{\pi^2}\frac{2m(2\pi\zeta)}{\rho D_{\text{mean}}^2}$	128.95	334.98	416.82

Table 2
Comparison of the force measurement results of the cantilever supported cylinder with the built-in supported cylinder at $\text{Re} = 3.0 \times 10^4$

Cylinder	Built-in support		Cantilever support	
	C_D	C'_L	C_D	C'_L
Wavy model 1	0.96	0.10	0.96	0.08
Wavy model 2	1.07	0.09	1.01	0.07
Wavy model 3	0.88	0.11	0.93	0.09

Therefore, a new normalized parameter, $a^2/(\lambda D_{\min})$, was proposed, which is used to express the degrees of cylinder obliqueness. The geometric parameters of all cylinders are shown in Table 1.

Each cylinder was vertically installed in the wind tunnel in a cantilever manner. Through a hole in the upper plate of the wind tunnel, the model was fixed (built-in support). The hole was made slightly larger than the diameter of the test cylinder so that no tunnel vibrations could be transmitted to the test model. The free end of the model is positioned at 1.5 mm away from the tunnel floor. In order to compare the mean drag coefficient of the wavy cylinders with that of a circular cylinder, a circular cylinder model of 18 mm diameter and 590 mm long was also investigated. Using a vibrometer controller (Polytec, OFV 502) and a fiber interferometer (Polytec, OFV 3001), the damping ratios ζ of all tested models were measured. The measured values and the corresponding mass ratio $m/\rho D_{\text{mean}}^2$ as well as the reduced damping parameter $2m(2\pi\zeta)/\pi^2\rho D_{\text{mean}}^2$ of the tested models are shown in Table 1. We can see that all the values of the reduced damping parameter are far greater than 10, which means that the vibration of the cylinders would be extremely small, even at resonance.

In order to estimate the effects of the inertia force on the experimental results, we compared the force measurement results of the cantilever cylinder with that of the rigid cylinder with both ends of the cylinder fixed (built-in support). The results are shown in Table 2. From the table, it can be seen that the mean drag is not affected by the presence of the small gap; the difference between the measurements is within the error margins of the experiment. On the other hand, the difference between the root-mean-square (r.m.s.) lift coefficients is as large as 20% or more. This is beyond measurement error and indeed shows a certain amount of inertia effect on the r.m.s. lift coefficient. However, as will be shown later, this inertia effect is not sufficient to mask the very drastic reduction measured on the r.m.s. lift coefficient from wavy cylinders. Therefore, it can be concluded that the effects of inertia force on the experimental results are not significant, and the unsteady forces measured are credible.

2.3. Load cell and its calibration

Numerous papers have examined the mean and fluctuating forces acting on cylinders in a cross-flow. Most investigators used surface pressure tapes to measure the pressure distribution around the cylinder (Farivar, 1981) and then integrated around the circumference to obtain the mean force. Shedden and Lin (1983) examined the drag force

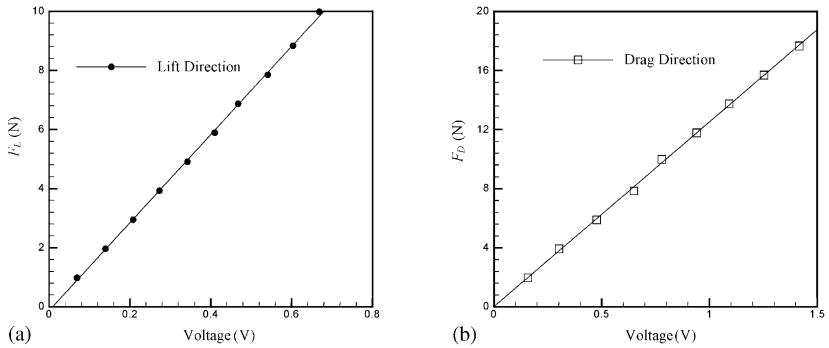

Fig. 2. Calibration results for the lift and drag force expressed linearly $F = -0.07 + 14.67V$ (lift-direction), $F = -0.01 + 12.50V$ (drag-direction).

fluctuation on a cylinder using a laser-cantilever force transducer. On the other hand, Sakamoto and Oiwake (1984) measured the mean and unsteady forces using a strain-gauge balance. Since the experiments were carried out using different diagnostic techniques and in different facilities with cylinder models having different stiffnesses, discrepancies were widely reported in the experimental data, especially for the unsteady force. So and Savkar (1981) measured the spanwise average unsteady force acting on a rigid cylinder in a turbulent stream directly using two piezoelectric three-axis load cells. Later, Sin and So (1987), Baban et al. (1989), Baban and So (1991), Fox and West (1993a, b) and West and Apelt (1997) measured the unsteady forces using similar sensors because the piezoelectric load cell method has the advantage of high resolution and small size as well as high stiffness. In view of these advantages, the present study also proposed to use this technique to measure the instantaneous integral forces acting on the wavy and circular cylinders.

A three-component quartz piezoelectric load cell (Kistler Model 9251A) was used as the sensing element. It was mounted to the test cylinder by a screw on the top end of the cylinder. One axis of the load cell was aligned to measure the pre-load applied along the axis of the cylinder. The other two axes (x, y) of the load cell were set to measure the instantaneous drag along the stream direction and the corresponding lift along the transverse direction. The electrostatic charge (pC) generated by the load cell is converted through a charge amplifier (Kistler Model 5011) into a proportional voltage, which was recorded by a computer data acquisition system. The load cell and the manner in which it was attached to the cylinder gave rise to very high stiffness. Therefore, the elastic properties of the cylinders do not affect the load cell measurement and vice versa. Cross-talk between the different axes and the temperature error of the load cell were minimized in order to optimize the measurement precision. Since the force components along x and y must be transmitted through friction in order to allow the tensile stresses to be measured, the load cell was preloaded along the z-axis to 100 kN. Thus configured, the forces along the x- and y-axis can be measured with accuracy. So and Savkar (1981) suggested that, if reasonably accurate force measurements were to be achieved, the pre-load/measured-load ratio has to be larger than six. The maximum measured force in the present experiment was about 10 N, thus giving a pre-load/measured-load ratio of 1.0×10^4. Therefore, the present arrangement is expected to yield fairly accurate measurements of the instantaneous force components. The load cell resolution is estimated to be 2 mN in the range, -10 to 10 N.

Static calibrations of the load cell in the lift and drag direction were carried out statically. A dead weight in the range of 0–20 N was used as the applied force. The calibration set-up is shown in Fig. 1. Since the load cell would be subjected to a bending moment, thus causing one of the three-direction outputs to increase and the other two to decrease, the calibration was carried out at every 100 mm along the span of the cylinder. A typical set of calibration curves are shown in Fig. 2. They were found to be linear and quite repeatable.

2.4. Pressure taps and hot-wire anemometry

Surface pressures were measured using 5 pressure taps on each wavy cylinder. The taps were spaced every 0.125λ, extending from a saddle to a node covering a distance of 0.5λ along the span. Tap 1 is located on a node and Tap 5 is located on a saddle. The diameter of each tap is 0.5 mm. The cylinders with 5 taps in the spanwise direction could be rotated from 0° to 360° with the aid of a movable plate. Anticlockwise rotation is taken to be positive. The mean surface pressure was measured every 10° using the electronic micromanometer.

In order to verify the spectral analysis results of the load cell signals and determine the vortex shedding frequency from the wavy cylinders, a hot-wire anemometer was also installed. It was mounted on an L-shape probe holder and

connected to a constant temperature anemometer (CTA), a filter amplifier and a data acquisition system. It was placed at $x = 1.6D_{max}$, $y = 2.0D_{max}$, and at different spanwise positions. The origin of x and y was taken to coincide with the cylinder center. Here, D_{max} is the maximum diameter of the cylinder models. Once the velocity signal was obtained, it was analyzed spectrally to give the dominant frequency. The Strouhal number obtained was compared with the load cell results.

2.5. Data recording

A UEI (United Electronics Industry) model WIN-30PGSH data acquisition system with sixteen analogue input channels was used to record all measurements. The maximum sampling rate of this system is 1.0×10^3 kHz. The hot-wire and load cell signals were properly conditioned by passing them through low-pass filters of 3 kHz before digitizing for analysis. In order to ensure sufficient data for later accurate analysis, a sampling rate of 20 kHz and a record length of 240 s were specified for each signal. This is sufficient to give accurate measurements of C'_L, the root mean square lift.

3. Results and discussion

In the following sections, results on the mean drag coefficient and pressure distribution are presented and analyzed first. The drag reduction effects of wavy cylinder of different degrees of obliqueness $a^2/(\lambda D_{min})$ are discussed. The fluctuating forces and the spectral contents of the force signals are then discussed and analyzed. This will help to gain further insight on the nature of fluctuating force reduction resulting from the three-dimensional surface geometry.

3.1. Mean drag coefficient and pressure distribution

3.1.1. Mean drag coefficient

The instantaneous force along the drag and lift direction of all the models was measured. Since all models were mounted in a cantilever manner with a gap between the free end of the model and the tunnel wall, experiments had been carried out to assess the effects of the gap on the measured forces. The spacing of the gap was varied from 1.5 to 5 mm under different free-stream velocities. No noticeable changes in the instantaneous force characteristics were observed. Therefore, it is assumed that the end effects of the gap on the measured forces and frequency spectra are negligible.

In order to measure the mean drag acting on the wavy and circular cylinders, two Kistler charge amplifiers (Type 5011) were used to convert the two measured directional electrical charges from the load cells into voltage signals. Due to low insulation resistance at the charge amplifier input, a slight drift at the output of the charge amplifier was detected. This drift signal increased with the time constant, especially when the time constant was large. On the other hand, zero offsets also existed in the experimental process, which could decrease the measurement precision. Therefore, it was necessary to eliminate the influence of drift and zero offset from the experimental data.

As the output voltage of the charge amplifier is directly related to the charge difference between two consecutive signals from the load cell, the steady force acting on the cylinder could only be calculated by recording the dynamic voltage change from $Re = 0$ to a definite Re. As an example of data processing in the experiments, a circular cylinder with 18 mm diameters and 590 mm length was considered. Re for this run is 2.3×10^4. The signals were recorded using the data acquisition system for 4 min (Fig. 3). Signals of the flow-induced lift and drag force during the first minute are

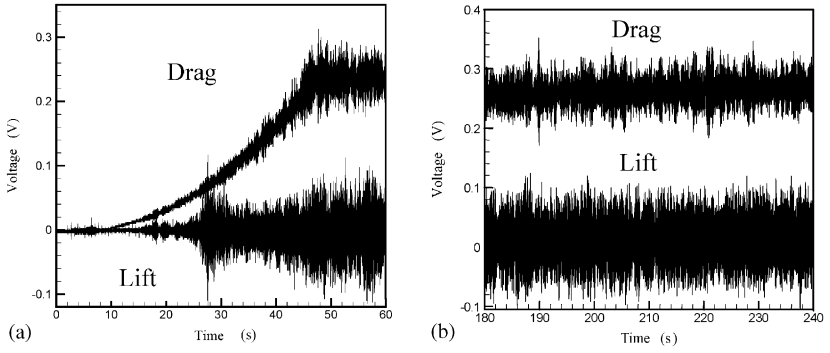

Fig. 3. Experimental force data of a circular cylinder with 18 mm diameter and 590 mm long at $Re = 2.3 \times 10^4$.

shown in Fig. 3(a), while Fig. 3(b) shows the result during the last minute. It can be seen that the transient period lasted for about 50 s after the wind tunnel was turned on. Therefore, the mean lift and drag could be determined by a linear fit of the data in the last minute. Using a polynomial fit, the zero-offset of the lift and drag signals can also be obtained. In order to verify the data processing method used in the current investigation, a comparison of the mean drag coefficient, $C_D = 2F_D/\rho U^2 LD$, thus measured with data reported in the literature is necessary. Here, F_D is the total mean drag force acting on the cylinder, L its length and ρ the fluid density. The well-documented data of C_D versus Re for a circular cylinder can be found in the studies of Wieselsberger (1921) and Roshko (1961). Since the data of Wieselsberger (1921) is fairly accurate and widely adopted, the present comparison is made with that data (Fig. 4). It can be seen that the two sets of data are in good agreement with each other. Therefore, it can be concluded that the processing method used to deduce C_D and the data thus obtained are fairly reliable.

The C_D of all wavy cylinder models and the circular cylinder are shown in Fig. 5 for a Re range of 2.0×10^4 to 5.0×10^4. From Fig. 5, it can be observed that the C_D of all wavy cylinder models is less than that of the corresponding circular cylinder. For example, when $\mathrm{Re} = 4.0 \times 10^4$, the C_D of models 1, 2 and 3 are equal to 0.9644, 1.028 and 0.9664, respectively, compared to a value of 1.1989 for the circular cylinder. This latter value is larger than that for the wavy cylinder models by about 19.6%, 14.3% and 19.4%, respectively. At other Re the amount of drag reduction is

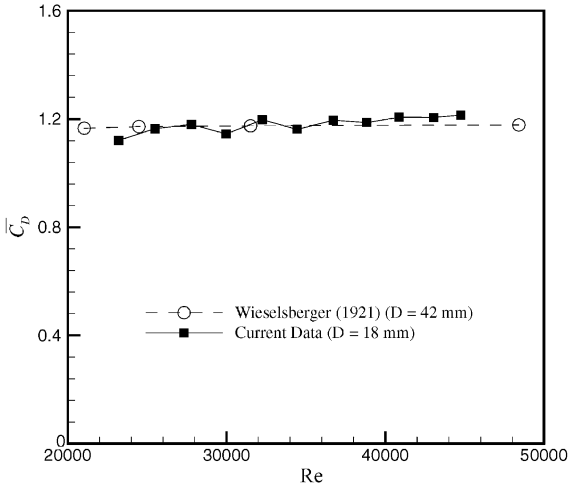

Fig. 4. Mean drag coefficient for a circular cylinder as a function of Re, dash line is the data from Wieselsberger (1921).

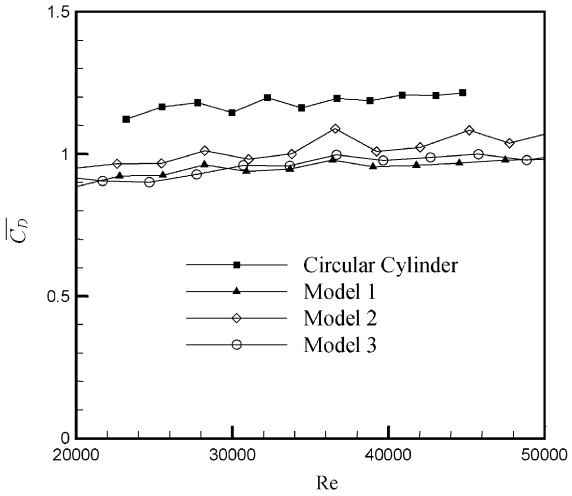

Fig. 5. Comparison of mean drag coefficient between the wavy cylinders and the circular cylinder for the $\mathrm{Re} = 2.0 \times 10^4$–$5.0 \times 10^4$.

essentially similar. This could be interpreted as a consequence of the base pressure of the wavy cylinders being higher than that of the circular cylinder. Another observation is that the C_D of model 2 is largest among all wavy cylinder models, while the C_D of model 1 and 3 is about the same. This trend is also reflected in the surface pressure distribution results.

3.1.2. Mean pressure distribution

To show the effect of geometry of the wavy curve on the static pressure distribution, the circumferential pressure distributions for all models at $\mathrm{Re} = 3.6 \times 10^4$ are plotted together in Fig. 6. In order to compare their behavior with that for a circular cylinder, the C_p distribution of a right circular cylinder at $\mathrm{Re} = 3.5 \times 10^4$ by Lam and Fang (1995) is also shown in Fig. 6. From the figure, it is evident that the separation at the saddle (tap 5) is much earlier than at the node (tap 1) for all wavy cylinder models. These effects become more evident as $a^2/(\lambda D_{\min})$ increases. For example, the separation of model 3 is earlier than that of model 1 and the latest separation occurs at the saddle of model 2. The maximum negative pressure coefficient shifts from $\theta = 60^\circ$ at the saddle to about 70° at the node. At a similar Re, the maximum negative pressure coefficient of the circular cylinder occurs at $\theta = 70^\circ$, which is slightly larger than those observed for wavy cylinders. The phenomenon shows that there is a significant unsteady three-dimensional flow around wavy cylinder at 60°–90°. From the figure, it is found that the circumferential pressure distribution of the wavy cylinder changes along its span. For all wavy cylinder models, the base pressure of the nodes (tap 1) is less than that of the saddles (tap 5). However, all the base pressures of the wavy cylinders are higher than that of the circular cylinder. The mean drag C_D is due to the pressure exerted on the upstream and downstream side of the cylinder. The former changes negligibly in the subcritical regime and hence C_D is proportional to C_{pb}. That is, the C_D of the wavy cylinders is less than that of the circular cylinder. This result also verified the results of mean force measurements by the load cell.

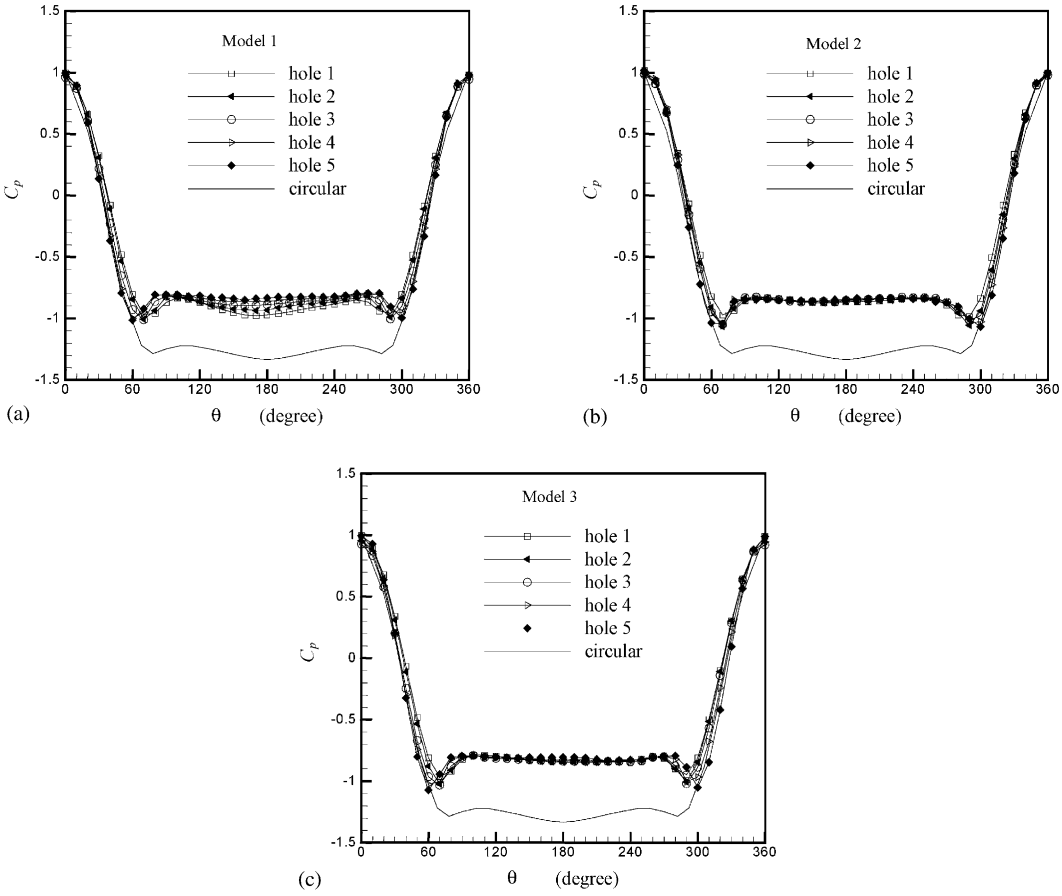

Fig. 6. Pressure coefficient distribution of model 1 (a), model 2 (b) and model 3 (c), respectively, $\mathrm{Re} = 3.6 \times 10^4$.

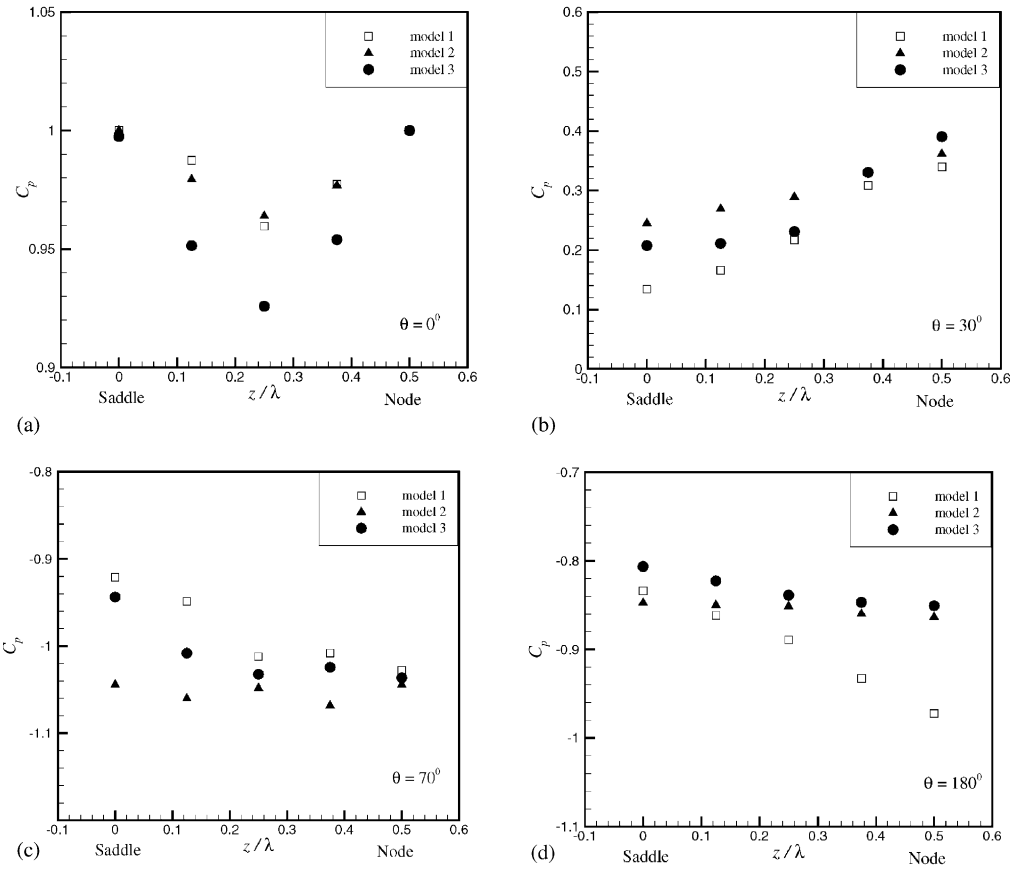

Fig. 7. Variations of mean pressure coefficient along the spanwise direction at various angular locations, $\mathrm{Re} = 3.6 \times 10^4$.

The variations of mean pressure coefficient along the spanwise direction at various angular locations are shown in Fig. 7. From Fig. 7(a) ($\theta = 0^\circ$), it can be found that C_p at the stagnation points (saddles and nodes) is about 1.0 for each cylinder, while at other spanwise locations C_p is less than 1.0. The minimum values of the C_p are located midway between the saddles and nodes. At $\theta = 30^\circ$ (Fig. 7(b)) the spanwise pressure gradient is positive from the saddle to the node. The gradient of model 3 is the largest, while the gradient of model 2 is the smallest. For each model, the gradient increases with θ until $\sim 40^\circ$, where the largest gradient occurs. For θ between 40° and 70°, the difference between the maximum and minimum C_p decreases. At $\theta \sim 70^\circ$, as shown in Fig. 7(c), C_p along the span is close to uniform, especially for model 2. As θ exceeds 70°, the variation of C_p along the span begins to reach a fairly uniform level, indicating boundary layer separation. For $\theta = 100^\circ - 160^\circ$, there are no discernible variations of spanwise C_p distribution. For $\theta = 170^\circ - 190^\circ$, there was a negative pressure gradient from saddle to node. The largest negative pressure gradient appears at $\theta = 180^\circ$, shown in Fig. 7(d). From above discussion, it is evident that the variation of C_p along the span is fairly sensitive to the geometry of the cylinders. In the present investigation, a dimensionless parameter, $a^2/(\lambda D_{\min})$, is introduced to describe the "degree of obliqueness" of the wavy cylinders (Table 1) with maximum value for model 3 and minimum value for model 2. For the tested wavy cylinder models, it is found that the C_p variation of model 3 along the span is the largest while the C_p variation of model 2 is the smallest. This trend is consistent with the obliqueness of the model.

3.2. Fluctuating forces and spectral analysis

3.2.1. Fluctuating lift and drag force coefficients

The variations of r.m.s. lift coefficient C'_L versus Re are shown in Fig. 8. It can be seen that the values of C'_L for all the wavy cylinder models are around 0.1 with a minimum value of 0.05 and a maximum value of about 0.2. Recently,

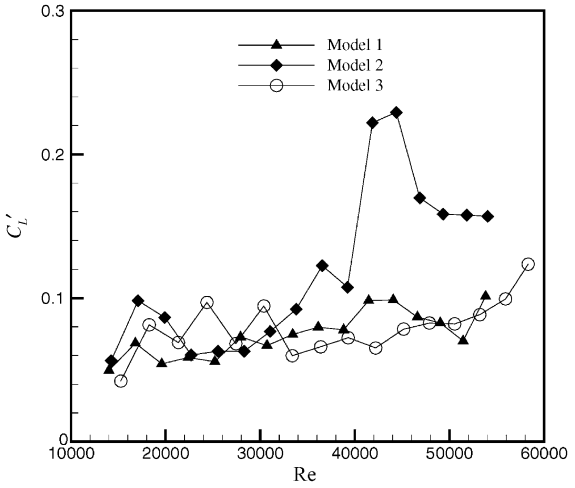

Fig. 8. RMS lift and drag of the wavy cylinder models versus Reynolds number.

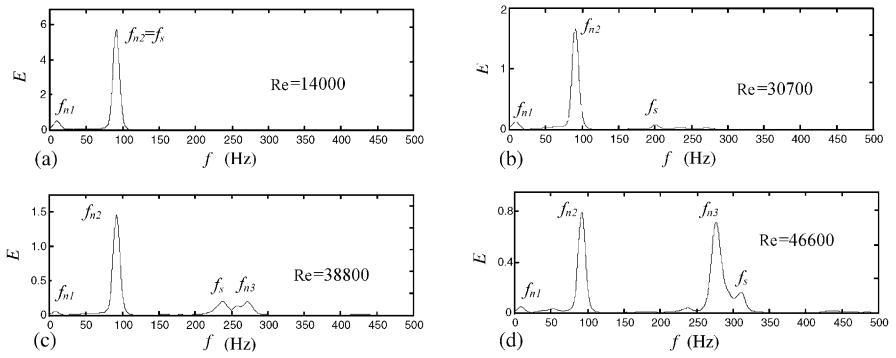

Fig. 9. Spectral analysis of the lift force for wavy cylinder model 1: (a) $\mathrm{Re}=1.4\times10^4$; (b) $\mathrm{Re}=3.07\times10^4$; (c) $\mathrm{Re}=3.88\times10^4$; and (d) $\mathrm{Re}=4.66\times10^4$.

Norberg (2001) summarized the previous results on lift coefficients of circular cylinders and found that C_L' varies from about 0.4 to 0.6 in the range of $\mathrm{Re}=1\times10^4$–5×10^4. These values are much greater than that of the wavy cylinders obtained here. From the figure, it is also noted that the variation of C_L' for the wavy model 2 with Re is much more drastic than that of the others. A small peak appears at about $\mathrm{Re}=4.4\times10^4$ for model 2, where the values of C_L' is about 0.22. The peak was due to the occurrence of resonance. This point will become clearer when the spectral analysis of C_L' for the wavy cylinders is examined. There it can be seen that as Re increases, the shedding frequency f_s also increases and resonance occurs as f_s approaches the natural frequency of the different modes of vibration of the cylinder, f_{ni}. For models 1 and 3, no such steep variations can be observed, even at a Re where resonance is expected. These results show that a wavy cylinder with a suitable geometry is capable of reducing the fluctuating lift even at or near resonance conditions. In this case, it appears that models 1 and 3 have a more stable behavior than model 2. The obliqueness of model 2 is the smallest, which means that the surface curve of model 2 is smoother than the others. Therefore, the three-dimensional characteristics in the wakes of models 1 and 3 might be stronger than that of model 2. This is why results for models 1 and 3 show a large effect on drag and lift reduction, while the behavior of model 2 is closest to that of the circular cylinder.

3.2.2. *Spectral analysis of the load cell signals*

The variations of the power spectral density (PSD) of C_L' are shown in Figs. 9 to 11. In order to identify the peak values in these figures, bump tests for every cylinder model were carried out. From the results, the natural frequencies of the test models shown in Table 1 are determined.

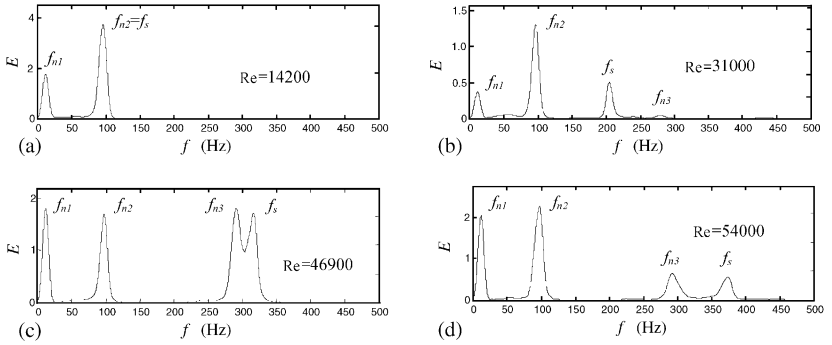

Fig. 10. Spectral analysis of the lift force for wavy cylinder model 2: (a) $\mathrm{Re} = 1.42 \times 10^4$; (b) $\mathrm{Re} = 3.1 \times 10^4$; (c) $\mathrm{Re} = 4.69 \times 10^4$; and (f) $\mathrm{Re} = 5.4 \times 10^4$.

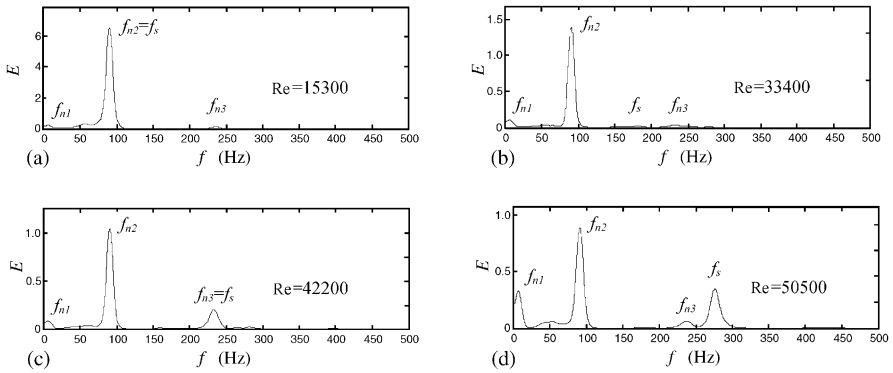

Fig. 11. Spectral analysis of the lift force for wavy cylinder model 3: (a) $\mathrm{Re} = 1.53 \times 10^4$; (b) $\mathrm{Re} = 3.34 \times 10^4$; (c) $\mathrm{Re} = 4.22 \times 10^4$; and (d) $\mathrm{Re} = 5.05 \times 10^4$.

From these figures, it can be clearly seen that f_s increases with increasing Re. The values of f_s are equal to those determined from the spectral analysis of the hot-wire signals measured at the same Re. In the present set-up, the first-mode natural frequencies of the models are always lower than the vortex shedding frequencies. As a result, resonant vibrations could only occur at the second and third mode natural frequencies of the models. The figures showed the changes of the peak mode shape as the vortex shedding frequency f_s passes and merges with the second and third mode natural frequency. For instance, Fig. 9(a) shows a very prominent peak around $\mathrm{Re} = 1.4 \times 10^4$. At this Re, the f_s and f_{n2} of the model 1 are approximately equal, indicating the occurrence of resonance. At other Re, for example, $\mathrm{Re} = 3.88 \times 10^4$ in Fig. 9(c), it is clear that the PSD values at the shedding frequency and other frequency components are much smaller than Fig. 9(a) case. For wavy cylinder models 1 and 3 (shown in Figs. 9 and 11, respectively), only the second mode natural frequency can be easily identified except at or near resonance. However, the spectra for model 2 (Fig. 10) show more peaks. Therefore, from these figures, it can also be found that wavy cylinder models 1 and 3 display a large fluctuating lift reduction.

3.2.3. *Strouhal number variation*

The vortex shedding frequencies f_s were both obtained from the spectral analysis of the hot-wire signal and from the load cell signals. The spectral analysis was performed using MATLAB and f_s are determined from the spectral density plots. The vortex shedding frequencies were also measured by the hot-wire anemometer in the wake of the wavy cylinders at three spanwise positions (node, saddle and middle) and are plotted in Fig. 12. From the figure, only one predominant frequency can be found for all tested models. The value of St is around 0.2 at all the spanwise positions. Hence drag reduction for wavy cylinder is not due to the variation of St unlike the results of Bearman and Tombazis (1993) and Tombazis and Bearman (1997) as well as Bearman and Owen (1998). In their investigations of wavy blunt-based section, they found that two distinct shedding frequencies emerged, and this ultimately leads to increased base

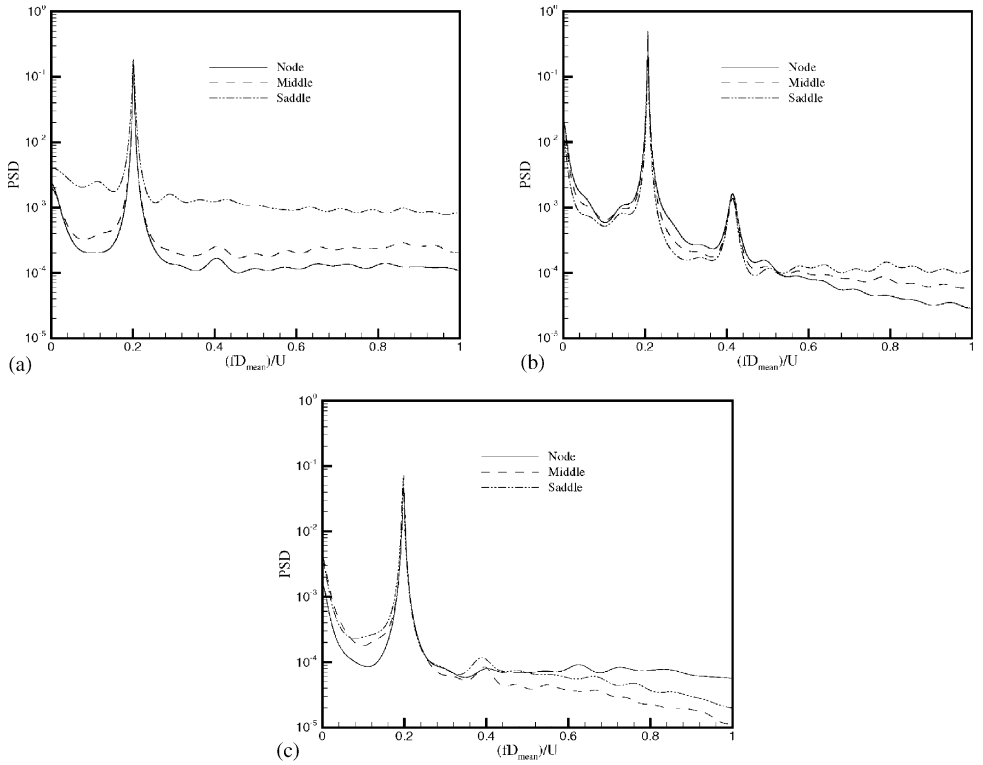

Fig. 12. Velocity power spectra measured at various spanwise position in the wake of the wavy cylinders, $\mathrm{Re} = 1.70 \times 10^4$. (a) Model 1; (b) model 2; and (c) model 3.

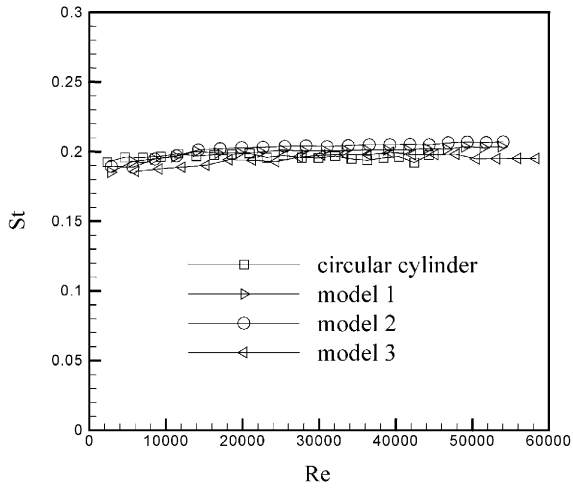

Fig. 13. Strouhal number of the circular and the wavy cylinders versus Re.

pressure. However, in the present study, we cannot find this two distinct shedding frequencies phenomenon in the spectral analysis of the hot-wire signals. The reason for this is not clear at present, but it is reasonable to believe that the drag and the fluctuating lift reduction of the wavy cylinder are independent of the vortex shedding behavior.

The plot of St ($= f_s D_{\mathrm{mean}}/U$) versus Re for all cylinder models is shown in Fig. 13. Here, D_{mean} is the mean diameter of the cylinder and U is the free-stream velocity. Because the results on the f_s using two methods are the same, only the

values obtained from the load cell signals are presented. The results show that the load cell signals are reliable for the monitoring of Strouhal periodicity due to vortex shedding. From Fig. 13, it can be seen that the St of all cylinder models has similar characteristics. That is, as Re increases from below 1.0×10^4 to about 6.0×10^4, St has no significant variation and only varies between 0.19 and 0.20. Therefore, it can be concluded that all cylinder models tested give essentially identical St versus Re distribution. In other words, variation in surface geometry has little or no effect on the formation of matured vortex shedding behind the cylinders. These results and those presented earlier suggest that the three-dimensional nature of the wake vortex is different for different cylinder models, or a re-organization of the wake structure due to surface geometry variation may be the main reasons for the drag and lift reduction and not due to the variation of Strouhal periodicity.

4. Conclusions

In this paper, we have studied the effects of three-dimensional geometric variation of wavy cylinders on drag reduction, vortex shedding and fluctuating force reduction. Experimental results including the mean and fluctuating force, the pressure distributions as well as the spectral analysis of the load cell signals and the hot-wire signals are presented.

Results for the mean drag coefficient indicate that the mean drag coefficients of the wavy cylinders are less than that of the circular cylinder with Re ranging from 2.0×10^4 to 5.0×10^4. A drag reduction of up to 20% can be achieved depending on the degree of obliqueness $a^2/(\lambda D_{\min})$ of the wavy cylinder. The pressure distributions indicated that the base pressure of the wavy cylinders at any spanwise location is higher than that of the circular cylinder at the same Re. Such results further support that the wavy cylinders display drag reduction. Furthermore, the variation of pressure coefficients along the spanwise direction at the same θ is fairly sensitive to the geometry of the wavy cylinders. There is a more rapid pressure drop and an earlier separation at the geometric saddle than at other spanwise locations for wavy cylinders. These effects become more evident as the degree of obliqueness $a^2/(\lambda D_{\min})$ increases.

The fluctuating force results show that the fluctuating lift coefficients of the wavy cylinders are lower than that of circular cylinders. It also indicates that the fluctuating force characteristics of the wavy cylinders are more incoherent than for a circular cylinder, and a wavy cylinder with a suitable geometric parameter $a^2/(\lambda D_{\min})$ is capable of reducing the fluctuating lift even at or near resonance conditions and eventually lead to the suppression of flow-induced vibration. Finally, velocity power spectra measured for the three spanwise positions, including a node, a saddle and the mid-point, show that there is no variation of the vortex shedding frequency along the spanwise direction of the wavy cylinder; the Strouhal number in the range of $\mathrm{Re} = 1.0 \times 10^4$–$6.0 \times 10^4$ is around 0.2, which equal to the values of circular cylinder.

Acknowledgements

This work was fully supported by a grant from the Research Grants Council of the Hong Kong Special Administrative Region, China (Project No. PolyU 5154/00E).

References

Ahmed, A., Bays-Muchmore, B., 1992. Transverse flow over a wavy cylinder. Physics of Fluids A 4, 1959–1967.

Ahmed, A., Khan, M.J., Bays-Muchmore, B., 1993. Experimental investigation of a three-dimensional bluff-body wake. AIAA Journal 31, 559–563.

Baban, F., So, R.M.C., 1991. Aspect ratio effect on flow-induced forces on circular cylinders in a cross-flow. Experiments in Fluids 10, 313–321.

Baban, F., So, R.M.C., Ötügen, M.V., 1989. Unsteady forces on circular cylinders in a cross-flow. Experiments in Fluids 7, 293–302.

Bearman, P.W., 1965. Investigation of the flow behind a two-dimensional model with a blunt trailing edge and fitted with splitter plates. Journal of Fluid Mechanics 322, 215–241.

Bearman, P.W., Tombazis, N., 1993. The effect of three-dimensional imposed disturbances on bluff body near wake flows. Journal of Wind Engineering and Industrial Aerodynamics 49, 339–350.

Bearman, P.W., Owen, J.C., 1998. Suppressing vortex shedding from bluff bodies by the introduction of wavy separation lines. Proceedings of the 1998 ASME Fluids Engineering Division Summer Meeting, FED-Vol. 245, Washington, DC, Session 191-09, FEDSM98-5190.

Blevins, R.D., 1994. Flow-Induced Vibration 2nd Edition. Krieger Publishing Company, Malabar, FL, USA.

Cooke, J.C., Robins, A.J., 1970. Boundary-layer flow between nodal and saddle points of attachment. Journal of Fluid Mechanics 41, 823–835.

Davey, A., 1961. Boundary-layer flow at a saddle point of attachment. Journal of Fluid Mechanics 10, 593–610.

Duck, P.W., 1979. Flow induced by a torsionally oscillating wavy cylinder, Quarterly Journal of Mechanics and Applied Mathematics, 32, No. 1, 73–91.

Farivar, D., 1981. Turbulent uniform flow around cylinders of finite length. AIAA Journal 19, 275–281.

Fox, T.A., West, G.S., 1993a. Fluid-induced loading of cantilevered circular cylinders in a low-turbulence uniform flow. Part 1: mean loading with aspect ratios in the range 4–30. Journal of Fluids and Structures 7, 1–14.

Fox, T.A., West, G.S., 1993b. Fluid-induced loading of cantilevered circular cylinders in a low-turbulence uniform flow. Part 2: fluctuating loads on a cantilever of aspect ratios 30. Journal of Fluids and Structures 7, 15–28.

Hover, F.S., Techet, A.H., Triantafyllou, M.S., 1998. Forces on oscillating uniform and tapered cylinders in crossflow. Journal of Fluid Mechanics 363, 97–114.

Keser, H. İbrahim, Ünal, M. Fevzi, Bearman, P.W., 2001. Simulation of wake from a circular cylinder with spanwise sinusoidal waviness. Proceedings of the Second International Conference on Vortex Methods, Istanbul, Turkey, September 26–28, 2001, pp. 131–137.

von Kerczek, C., 1988. The symmetry plane boundary layer on a corrugated cylinder in cross flow. AIAA Paper No. AIAA-88-3544-CP.

Lam, K., Fang, X., 1995. The effect of interference of four equispaced cylinders in cross flow on pressure and force coefficients. Journal of Fluids and Structures 9, 195–214.

Norberg, C., 2001. Flow around a circular cylinder: aspects of fluctuating lift. Journal of Fluids and Structures 15, 459–469.

Nuzzi, F., Magness, C., Rockwell, D., 1992. Three-dimensional vortex formation from an oscillating, non-uniform cylinder. Journal of Fluid Mechanics 238, 31–54.

Petrusma, M.S., Gai, S.L., 1994. The effect of geometry on the base pressure recovery of segmented blunt trailing edges. Aeronautical Journal 98, 267–274.

Petrusma, M.S., Gai, S.L., 1996. Bluff body wakes with free, fixed, and discontinuous separation at low Reynolds numbers and low aspect ratio. Experiments in Fluids 20, 189–198.

Rodriguez, O., 1991. Base drag reduction by control of the three-dimensional unsteady vortical structures. Experiments in Fluids 11, 218–226.

Roshko, A., 1961. Experiments on the flow past a circular cylinder at very high Reynolds number. Journal of Fluid Mechanics 10, 345–356.

Sakamoto, H., Oiwake, S., 1984. Fluctuating forces on a rectangular prism and a circular cylinder placed vertically in a turbulent boundary layer. ASME Journal of Fluids Engineering 106, 160–166.

Sakamoto, H., Haniu, H., 1994. Optimum suppression of fluid forces acting on a circular cylinder. ASME Journal of Fluids Engineering 116, 221–227.

Shedden, R., Lin, S.P., 1983. Drag-force fluctuation on a cylinder. Journal of Fluid Mechanics 127, 443–452.

Sin, V.K., So, R.M.C., 1987. Local force measurement on finite span cylinders in a cross-flow. ASME Journal of Fluids Engineering 109, 136–143.

So, R.M.C., Savkar, S.D., 1981. Buffeting forces on rigid circular cylinders in cross flows. Journal of Fluids Mechanics 105, 397–425.

Tombazis, N., Bearman, P.W., 1997. A study of three-dimensional aspects of vortex shedding from a bluff body with a mild geometric disturbance. Journal of Fluid Mechanics 330, 85–112.

West, G.S., Apelt, C.J., 1997. Fluctuating lift and drag forces on finite lengths of a circular cylinder in the subcritical Reynolds number range. Journal of Fluids and Structures 11, 135–158.

Wieselsberger, C., 1921. Neuere festellungen über die Gesetze des Flüssigkeits und Luftwider-standes. Physikalische Zeitschrift 22, 321–328.